REVIEW
SOLID EARTH: GEOMAGNETISM

Earth and Planetary Physics
8: 445–458, 2024
doi: 10.26464/epp2024025

Preliminary geological interpretation of long-wavelength magnetic anomalies over China and surrounding regions

Jie Wang[1*], YanYan Yang[1*], ZhiMa Zeren[1], Jian Wang[1,2], Xin Wang[1], YuXin Luo[1,3], and XuHui Shen[4]

[1]National Institute of Natural Hazards, Ministry of Emergency Management of China, Beijing 100085, China;

[2]Key Laboratory of Compound and Chained Natural Hazards Dynamics, Ministry of Emergency Management of China, Beijing 100085, China;

[3]School of Emergency Management Science and Engineering, University of Chinese Academy of Sciences, Beijing 100049, China;

[4]National Space Science Center, Chinese Academy of Sciences, Beijing 100190, China

Key Points:

- Geological origins of long-wavelength magnetic anomalies in China and surrounding regions are reviewed, including six magnetic high anomalies over the (1) Tarim Basin, (2) Sichuan Basin (3) Great Xing'an Range, (4) Barmer Basin, (5) Central Myanmar Basin, and (6) Sunda and Banda Arcs, and a striking magnetic low anomaly along the southern part of the Himalayan-Tibetan Plateau.
- The tectonic backgrounds for these long-wavelength anomalies are related to either ancient basin basement or subduction-collision zone.
- The difficulties of geological interpretation of long-wavelength magnetic anomalies come mainly from limited surface exposure of sources, later tectonic destruction, and superposition of multi-phase events.

Citation: Wang, J., Yang, Y. Y., Zeren, Z. M., Wang, J., Wang, X., Luo, Y. X., and Shen, X. H. (2024). Preliminary geological interpretation of long-wavelength magnetic anomalies over China and surrounding regions. *Earth Planet. Phys.*, *8*(3), 445–458. http://doi.org/10.26464/epp2024025

Abstract: Long-wavelength (>500 km) magnetic anomalies originating in the lithosphere were first found in satellite magnetic surveys. Compared to the striking magnetic anomalies around the world, the long-wavelength magnetic anomalies in China and surrounding regions are relatively weak. Specialized research on each of these anomalies has been quite inadequate; their geological origins remain unclear, in particular their connection to tectonic activity in the Chinese and surrounding regions. We focus on six magnetic high anomalies over the (1) Tarim Basin, (2) Sichuan Basin (3) Great Xing'an Range, (4) Barmer Basin, (5) Central Myanmar Basin, and (6) Sunda and Banda Arcs, and a striking magnetic low anomaly along the southern part of the Himalayan-Tibetan Plateau. We have analyzed their geological origins by reviewing related research and by detailed comparison with geological results. The tectonic backgrounds for these anomalies belong to two cases: either ancient basin basement, or subduction-collision zone. However, the geological origins of large-scale regional magnetic anomalies are always subject to dispute, mainly because of limited surface exposure of sources, later tectonic destruction, and superposition of multi-phase events.

Keywords: long-wavelength magnetic anomaly; lithospheric magnetic anomaly; lithospheric magnetic field model; satellite magnetic survey; CSES

1. Introduction

Long-wavelength magnetic anomalies with resolution in hundreds of kilometers were first found in satellite magnetic surveys. Magnetic scalar data from the POGO satellite series (1967–1971) first confirmed that weak long-wavelength magnetic anomalies appeared to originate in the Earth's lithosphere; POGO data were used to derive the first global magnetic anomaly map (Figure 1a; Regan et al., 1975). The Magsat satellite (1979–1980) was designed to increase the resolution of magnetic detection; its data were used to produce global vector and scalar magnetic anomaly maps for geophysical studies (Figure 1b; Langel et al., 1982; Arkani-Hamed et al., 1994; Ravat et al., 1995; Langel and Hinze, 1998). After a gap of 20 years, data from the Danish Ørsted satellite (1999–2013) confirmed Magsat findings and led to realization that large-scale lithospheric magnetization is mainly induced (Purucker et al., 2002). In the same era the German CHAMP satellite (2000–2010) produced particularly valuable data for lithospheric field modeling; its low altitude (300 to 454 km) allowed stronger correlation with known geological and tectonic features (Figure 1c; Maus et al., 2002, 2008; Hemant and Maus, 2005). Data from the ESA's Swarm satellite constellation (2013–), which comprises three identical satellites (Friis-Christensen et al., 2006), has facilitated creation of various high-quality lithospheric field models (Thébault et al., 2016; Olsen et al., 2017). The CSES

Correspondence to: J. Wang, jiewang@ninhm.ac.cn
Y. Y. Yang, yanyanyang@ninhm.ac.cn
Received 01 FEB 2024; Accepted 01 APR 2024.
First Published online 07 MAY 2024.

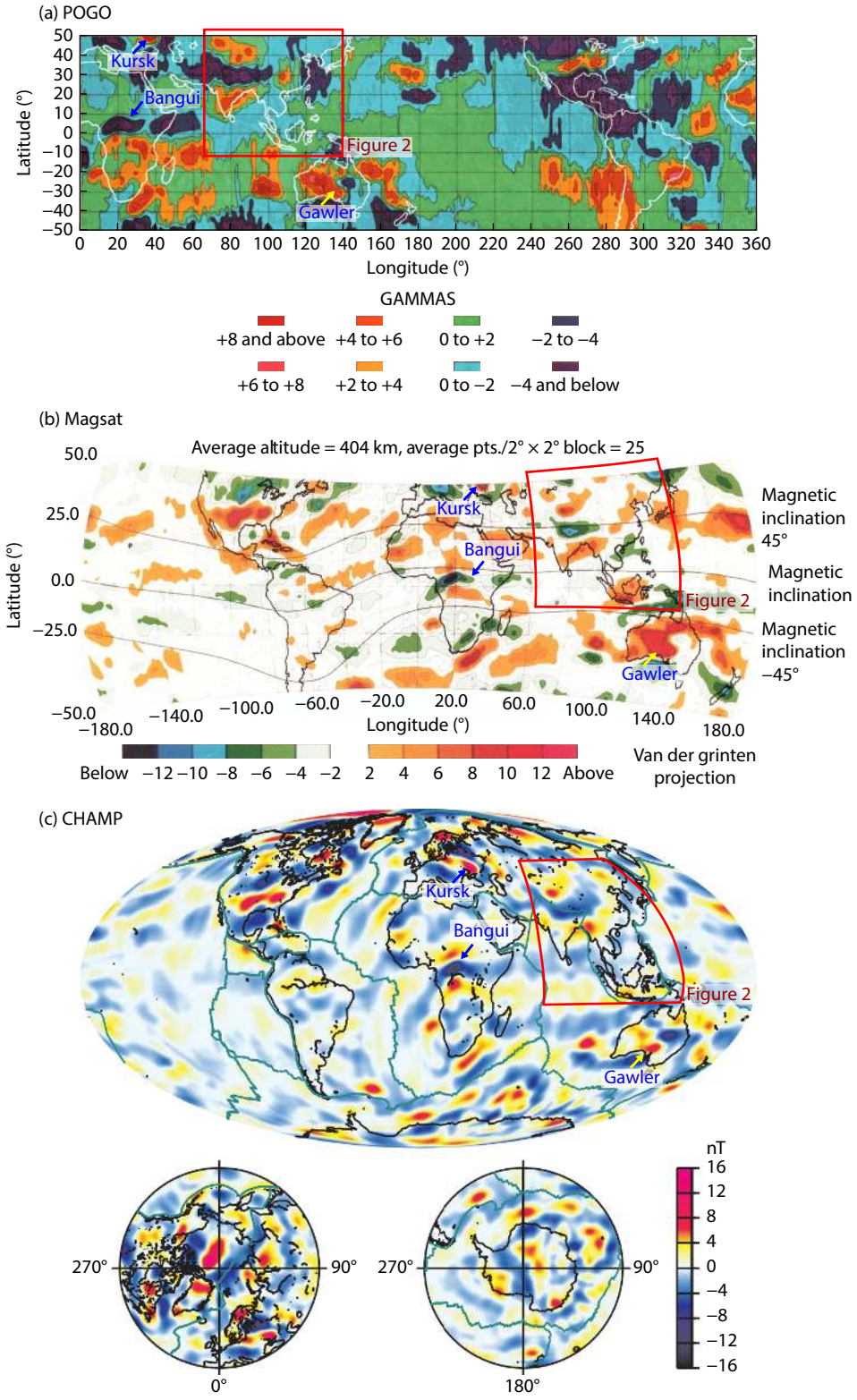

Figure 1. Global scalar magnetic anomaly map derived from (a) POGO data at a mean altitude of 540 km, modified from Regan et al. (1975); (b) Magsat data at a mean altitude of 404 km, modified from Langel et al. (1982); (c) CHAMP data at 438 km altitude, modified from Maus et al. (2002). The red box represents the range of Figure 2.

(China Seismo-Electromagnetic Satellite, 2018-) is designed to facilitate earthquake studies and to measure geophysical fields, supporting scientific goals of both space and solid earth physics (Shen XH et al., 2018; Huang JP et al., 2018); its scalar magnetic data have been used for lithospheric magnetic anomaly identification and modeling (Wang J et al., 2021, 2023a, b). In May 2023, a new Chinese satellite aiming at monitoring geomagnetic changes, the Macao Science 1 satellite (Zhang K K, 2023), was launched.

Furthermore, a subsequent CSES-02 satellite is planned to be launched in 2024.

Long-wavelength magnetic anomalies have been attributed to magnetized bodies deep in the lower crust, but also locally, to the uppermost mantle (Ferré et al., 2014). Interpretations of lithospheric magnetic anomalies have been used in geological mapping, in determination of crustal composition and structure, in plate tectonic reconstruction, and in geodynamics (Purucker and Clark, 2011). But due to limited exposure on the surface, the geological origins of long-wavelength magnetic anomalies are always controversial.

Consider three examples:

(a) **The Bangui magnetic anomaly**. The first confirmation, in satellite data, of the existence of a long-wavelength magnetic anomaly with geological origin was the identification of the Bangui magnetic anomaly over central Africa (Regan et al., 1973). Its center is a prominent magnetic low located at 5°N latitude (Figure 1). It is in an area of highly metamorphosed Precambrian rocks, but does not correlate with any surface features. Regan and Marsh (1982) interpreted it to be caused by early intrusions in the crust, followed by subsidence and deformation. Another hypothesis (Girdler et al., 1992) is that the Bangui magnetic anomaly has an extra-terrestrial cause, i.e., impact origin.

(b) **The Kursk magnetic anomaly**. It is one of the largest-amplitude magnetic anomalies in Russia. In ground-based measurements, the maximum amplitude of the Kursk anomaly was found to be nearly 200,000 nT (Ravat et al., 1993; Taylor et al., 2014). The distribution of the Kursk magnetic anomaly is correlated with the large iron-ore deposit in the Voronezh Crystalline Massif of the Ukrainian Shield, a Precambrian basement structure (Ravat et al., 1993). While the exposed iron-rich formations extend only to a depth of 5 km, quantitative magnetic modeling of the Kursk anomaly calls for a still deeper source (Taylor and Frawley, 1987; Taylor et al., 2014).

(c) **The Gawler magnetic anomaly**. This large-scale satellite magnetic high anomaly is in south Australia. The Gawler craton is the conjugate continent margin of east Antarctica during the Gondwana reconstruction (Goodge and Finn, 2010). It comprises Archean to Mesoproterozoic rocks that have remained substantially undeformed since about 1450 Ma; much of the Gawler basement remains hidden by younger materials. Finn et al. (2006) thought that the anomaly was caused primarily by magnetite-rich Paleoproterozoic to Mesoproterozoic intrusions in the Gawler craton. von Frese et al. (2013) related it to a possible giant end-of-Permian impact in the east Antarctic, based on gravity and subglacial terrain data, and thought that this anomaly reflects the thermal enhancement, caused by the impact, of viscous remanent magnetization in the lower crust.

Compared to the more striking magnetic anomalies around the world, the long-wavelength magnetic anomalies in China and surrounding regions are much weaker, with maximum amplitudes of about 5 nT at 500 km altitude (Figure 2). Thanks to high-resolution magnetic measurements and mature modeling methods, many researchers have begun to notice these magnetic anomalies and have done general analyses using geological and tectonic data (An ZC et al., 1992; Zhang CD, 2003; Kang GF et al., 2010; Ou JM et al., 2013; Du JS, 2014; Gao GM et al., 2018; Wang J et al., 2020a, 2023a). However, specialized research on these weaker anomalies has been quite inadequate to clarify their geological origins or to facilitate further tectonic applications. To encourage greater research attention to the origins of the long-wavelength magnetic anomalies in China and surrounding regions, first, we have applied multiple geomagnetic field models and identified seven anomalies, including six magnetic high anomalies in the (1) Tarim Basin in the northwest of China, (2) Sichuan Basin in the southwest of China, (3) Great Xing'an Range in the northeast of China, (4) Barmer Basin in the northwest of India, (5) Central Myanmar Basin in Myanmar and (6) Sunda and Banda Arcs in Indonesia, and a magnetic low anomaly along the southern part of the Himalayan-Tibetan Plateau. We have then analyzed their geological origins, based on reviews of related research and detailed comparisons with geological data.

2. Long-wavelength Magnetic Anomalies Calculated by Multiple Models

In satellite magnetic measurements, the relatively weak lithospheric magnetic signal can be effectively hidden by the much stronger core field (generated by electrical currents in the liquid outer core), and the external field (related to current systems in the ionosphere and magnetosphere); moreover, residual error from the satellite platform or other sources can be of the same order of magnitude as the signal from small-scale anomalies. To assure that a weak long-wavelength magnetic anomaly can be detected and described, we chose four different lithospheric magnetic field models to create anomaly maps, and have focused only on anomalies whose amplitudes at 500 km altitude are greater than 2 nT.

2.1 Spherical Harmonic (SH) Analysis

The potential V of the lithospheric magnetic field $\boldsymbol{B} = -\nabla V$ satisfies Laplace's equation. In spherical coordinates, the solution of Laplace's equation can be expressed as a series of spherical harmonics:

$$V = a\sum_{n=1}^{N}\sum_{m=0}^{n}\left(\frac{a}{r}\right)^{n+1}\left(g_n^m\cos m\phi + h_n^m\sin m\phi\right)P_n^m(\cos\theta), \tag{1}$$

where a = 6371.2 km is the Earth's reference radius; (r, θ, ϕ) are radius, co-latitude, and longitude of the geocentric spherical coordinate system, respectively; g_n^m and h_n^m are the Gaussian spherical harmonic coefficients; N is the maximum degree of the Gauss coefficients; m and n are the order and degree of spherical harmonics; and P_n^m are the associated Schmidt semi-normalized Legendre functions.

2.2 Lithospheric Magnetic Field Models

To map and characterize magnetic anomalies over China and surroundings, we selected four lithospheric magnetic field models, the MF7 (Maus et al., 2008), the CM6 (Sabaka et al., 2020), the CHAOS-7 (Finlay et al., 2020) /LCS-1 (Olsen et al., 2017) and the CSES (Wang J et al., 2023b) models, all of which are derived from satellite data alone, without near-surface (aeromagnetic or

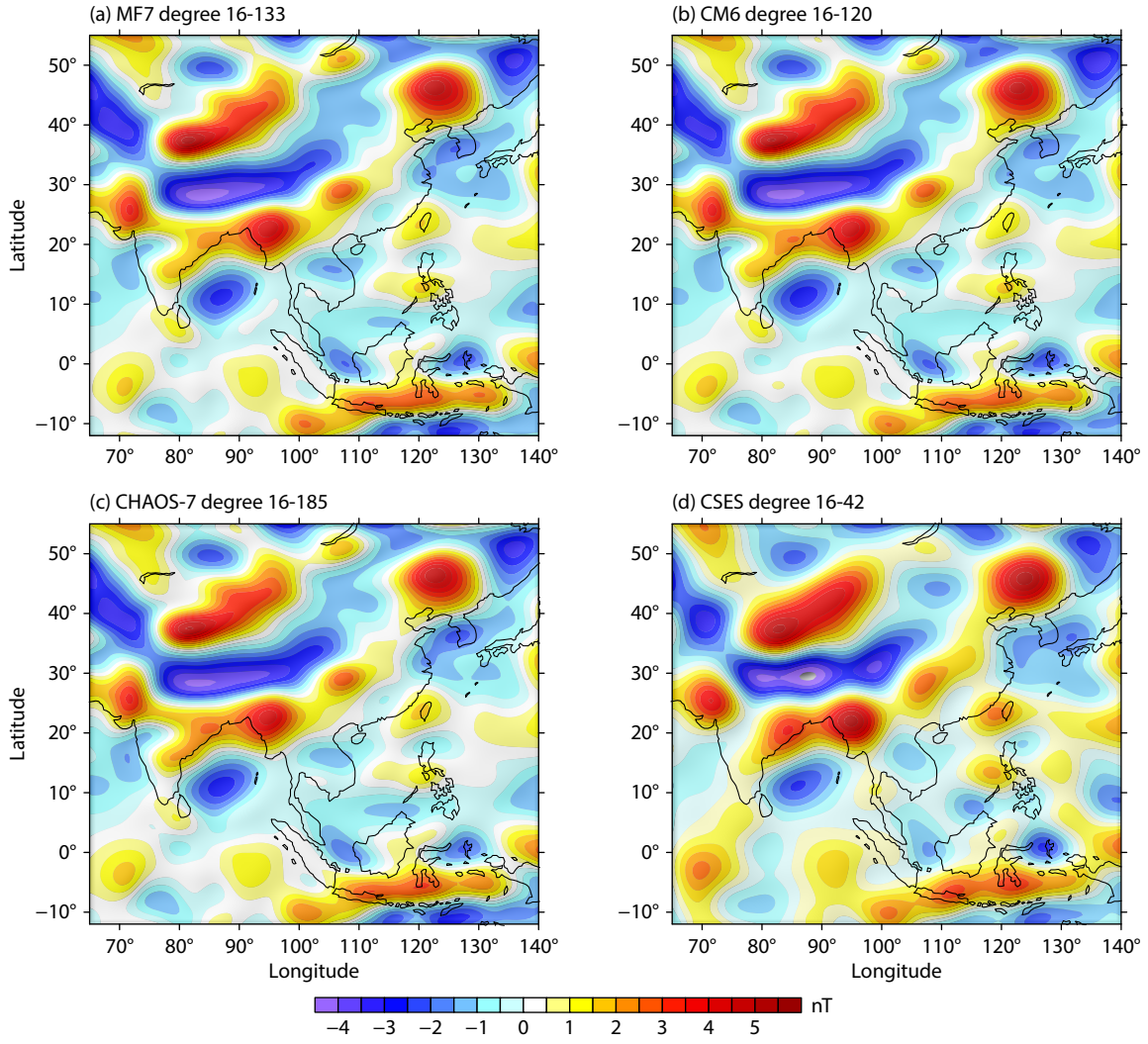

Figure 2. The long-wavelength magnetic anomaly map of China and surrounding regions calculated by four models: (a) the MF7, (b) the CM6, (c) the CHAOS-7, and (d) the CSES, all at 500 km altitude. The black curves are the coast lines.

Table 1. Lithospheric magnetic field model information.

Model	Maximum SH degree	Equivalent wavelength	Satellite data source	Website	Reference
MF7	133	300 km	CHAMP	https://geomag.colorado.edu/magnetic-field-model-mf7.html	Maus et al., 2008
CM6	120	333 km	Ørsted, SAC-C, CHAMP, and Swarm	http://www.spacecenter.dk/files/magnetic-models/CM6/	Sabaka et al., 2020
CHAOS-7/LCS-1	185	216 km	Ørsted, CHAMP, SAC-C, Cryosat-2 and Swarm	http://www.spacecenter.dk/files/magnetic-models/CHAOS-7/ http://www.spacecenter.dk/files/magnetic-models/LCS-1/	Finlay et al., 2020 Olsen et al., 2017
CSES	42	952 km	CSES	https://www.leos.ac.cn/#/article/info/250	Wang J et al., 2023b

marine) data, which means that the long-wavelength magnetic anomalies decay slowly. Table 1 presents brief descriptions of the four models.

The MF7 model (Maus et al., 2008) is obtained in a sequential approach using CHAMP satellite magnetic data (see https://geomag.colorado.edu/magnetic-field-model-mf7.html for model coefficients). It removes sequentially all other known magnetic field contributions, thus selecting data that are the least-contaminated by external field contributions. The results of this model have correlated well with geological features, and have even been able to resolve the direction of oceanic magnetic lineation, revealing the age structure of oceanic crust.

The CM6 model (Sabaka et al., 2020) was derived from more than 20 years of satellite data (from Ørsted, CHAMP, SAC-C, and

Swarm satellites) and ground-based observatory data (see http://www.spacecenter.dk/files/magnetic-models/CM6/ for model coefficients). CM6 is the first model to combine both CHAMP and Swarm data in a comprehensive approach that strives to invert, simultaneously, various datasets that capture, mathematically, all internal and external fields varying in space and time. The resulting core, lithosphere, oceanic tidal M2, ionosphere, magnetosphere, and associated induced magnetic field descriptions are in very good agreement with those derived previously from other models.

The CHAOS-7 model (Finlay et al., 2020) is based on satellite data from Ørsted, CHAMP, SAC-C, Cryosat-2, and the three Swarm satellites, as well as on monthly mean data recorded by a large group of ground magnetic observatories. It describes the core field, the external field, and the lithospheric field (see http://www.spacecenter.dk/files/magnetic-models/CHAOS-7 for model coefficients). Above degree 25, the lithospheric part of the CHAOS-7 model is the same as the LCS-1 model (Olsen et al., 2017). The LCS-1 model is derived from magnetic observations of the CHAMP and Swarm satellite (see http://www.spacecenter.dk/files/magnetic-models/LCS-1/ for model coefficients). It is determined entirely from magnetic "gradient" data (approximated by finite differences) and parametrized by equivalent point sources located at a depth of 100 km below the surface. In a final step the point-source representation is transformed to a spherical harmonic expansion. At low degrees, CHAOS-7 shows very good agreement with previous satellite-derived lithospheric field models. Comparison with independent near-surface aeromagnetic data from Australia yields good agreement at horizontal wavelengths up to degree 160.

The CSES model (Wang J et al., 2023b) is a global lithospheric magnetic field model between ±65° latitude for degrees 16–42; it was derived from CSES scalar magnetic data collected only from March 2018 to November 2022 (see https://www.leos.ac.cn/#/article/info/250 for model coefficients). Compared with the CHAOS-7, CM6, and MF7 models, CSES shows good agreement in terms of power spectra and anomaly details. However, due to the polar gaps and orbital gaps in the CSES data, the CSES lithospheric magnetic field model is reliable only up to spherical harmonic degree 42.

2.3 Long-wavelength Magnetic Anomalies at 500 km Altitude

It is to be noted that the magnetic anomaly T is not equal to the modulus (root mean square of the three components) of the lithospheric magnetic field. It is the modulus difference between the internal total field and the core field

$$T = |\boldsymbol{B}_{\rm core} + \boldsymbol{B}_{\rm litho}| - |\boldsymbol{B}_{\rm core}|, \tag{2}$$

where $|\boldsymbol{B}_{\rm core}|$ is the modulus of the core magnetic field and $|\boldsymbol{B}_{\rm core} + \boldsymbol{B}_{\rm litho}|$ is the modulus of the internal magnetic field (including the core and lithospheric magnetic field).

To show the major magnetic anomalies clearly, anomaly values (CHAOS-7 model result at 500 km altitude) in the range from −2 nT to 2 nT are displayed in grey color to filter out the lower

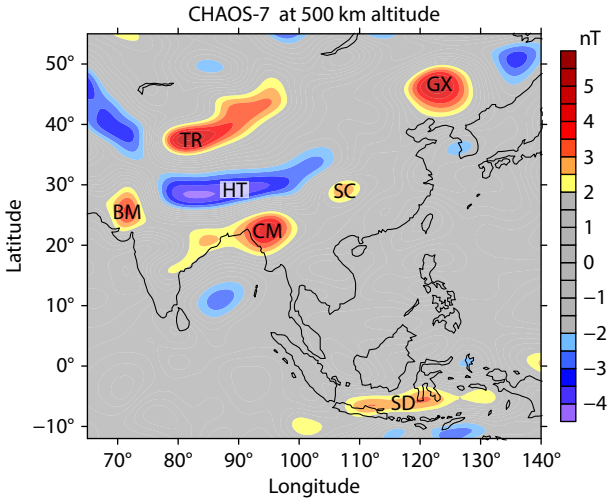

Figure 3. Major long-wavelength magnetic anomalies in China and surrounding regions. The contours are the lithospheric magnetic anomalies calculated via the CHAOS-7 model at 500 km altitude. Abbreviations: TR, Tarim Basin; SC, Sichuan Basin; GX, Great Xing'an Range; BM, Barmer Basin; CM, Central Myanmar Basin; SD, Sunda and Banda Arcs; HT, Himalayan-Tibetan Plateau.

amplitude anomalies. In Figure 3, six obvious magnetic high anomalies can be seen, located at (1) the Tarim Basin in the northwest of China (TR), (2) the Sichuan Basin in the southwest of China (SC), (3) the Great Xing'an Range in the northeast of China (GX), (4) the Barmer Basin in the northwest of India (BM), (5) the Central Myanmar Basin in Myanmar (CM) and (6) the Sunda and Banda Arcs in Indonesia (SD). Besides, there is a striking magnetic low anomaly along the southern part of the Himalayan-Tibetan Plateau (HT). In the next section we analyze, separately, the geological origins of these seven magnetic anomalies.

3. Geological Interpretations

In this section, we analyze separately the geological interpretations of the seven significant magnetic anomalies in China and surrounding regions. At the altitude of data-collection by low-earth-orbiting satellites, most details represented by high degree spherical harmonics decay quickly and become invisible, which makes it difficult to correlate these anomalies with geological and tectonic sources. Hence, Figure 4a presents the magnetic anomalies at the Earth's surface, as calculated using CHAOS-7 (the satellite-based model that includes the highest SH degree — up to 185), in order to display these anomalies in as much detail as the models allow. The long-wavelength CHAOS-7 magnetic anomaly maps at 100 km and 300 km altitudes (Figures 4b and 4c) are also calculated to show how the magnetic anomaly signals decay with altitude, which is helpful during spatial comparison with geological data. For ease of reference, Figure 2c, the CHAOS-7 anomaly map at 500 km altitude, is repeated as Figure 4d.

It is noted that, if we would like to compare magnetic anomalies with geological maps or other geodata, *Reduction To the Pole* (RTP) is necessary so that the magnetic anomalies can better reflect their source locations. In oblique magnetization (inclination $\neq 90°$), the locations of magnetic anomalies would shift laterally over the sources; the shape of magnetic anomalies would be

skewed (Blakely, 1995). RTP reduces the influences of oblique magnetization. For large-scale magnetic anomalies, position offsets caused by oblique magnetization could reach tens of kilometers, which would cause serious error when comparing a magnetic anomaly with geological maps, especially in complex tectonic settings. In this article, the RTP adjustment is carried out in the frequency domain: the RTP factor $H(u,v)$ is expressed as

$$H(u,v) = H(\theta) = \frac{1}{\left[\mathrm{i}\cos I_0 \cos(\theta - D_0) + \sin I_0\right]^2}, \tag{3}$$

where $\theta = \arctan\frac{u}{v}$, $\mathrm{i} = \sqrt{-1}$, I_0 is inclination, and D_0 is declination.

In low latitudes, a small I_0 would cause large $H(\theta)$ and make the RTP result unstable, causing stripe error along the declination trends. To reduce the instability of RTP at low latitudes, the RTP is processed with a suppression filter (Yao CL et al., 2003).

3.1 TR: Tarim Basin

The Tarim magnetic anomaly is located in northwest China, extending more than 1500 km, trending approximately E-W. This prominent high anomaly occupies the central and southern part of the Tarim Basin. The northern Tarim Basin shows no obvious high anomaly, which indicates significant difference between the North and South Tarim Basin. The Tarim has an ancient Precambrian basement, covered by sedimentary layers from late Neoproterozoic to Cenozoic, meaning that the Tarim Basin acts as a stable craton since the Neoproterozoic. Most surface areas of the Tarim basin are covered by desert (Figure 5a). The sedimentary rocks are commonly non-magnetic, except basic basalts. Although the Tarim Basin experienced some later reactivated magmatic events that produced basalt layers inside the basin, e.g., the Ordovician igneous bodies (He BZ et al., 2011) and the Permian Tarim LIP (large igneous province) (Yang SF et al., 2017), these extrusive igneous layers could not be sources of the observed large-scale Tarim magnetic anomaly. The reasons are: (1) spatial scale. The Tarim magnetic anomaly calls for a craton-scale source extending from the west to east edges of the Tarim Basin, but these reactivation activities influenced only part of the Tarim Basin, not the whole basin. (2) rock magnetization. The basalts have strong remanent magnetization with irregular magnetization directions, and their field values change in a wide range, so they often generate signals with drastic changes during near-surface magnetic surveys, which decay quickly with distance and contribute little to long-wavelength signals. Hence, the Tarim magnetic anomaly is likely to originate in the basin basement, and thus provides information primarily of the composition difference

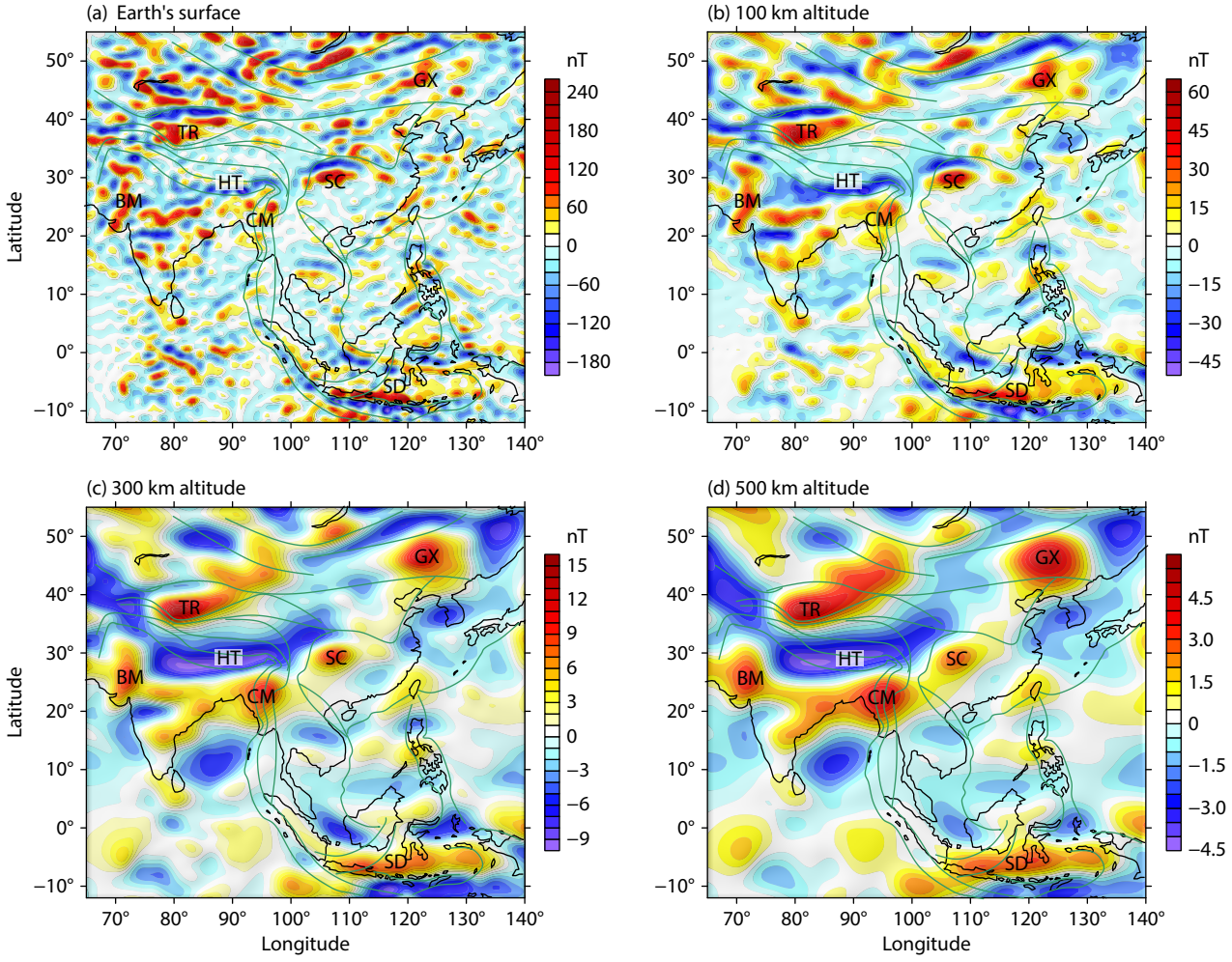

Figure 4. The lithospheric magnetic anomaly map at different altitudes, calculated by the CHAOS-7 model. The black curves are the coast lines. The green curves are the tectonic lines simplified from Ingram et al. (2004).

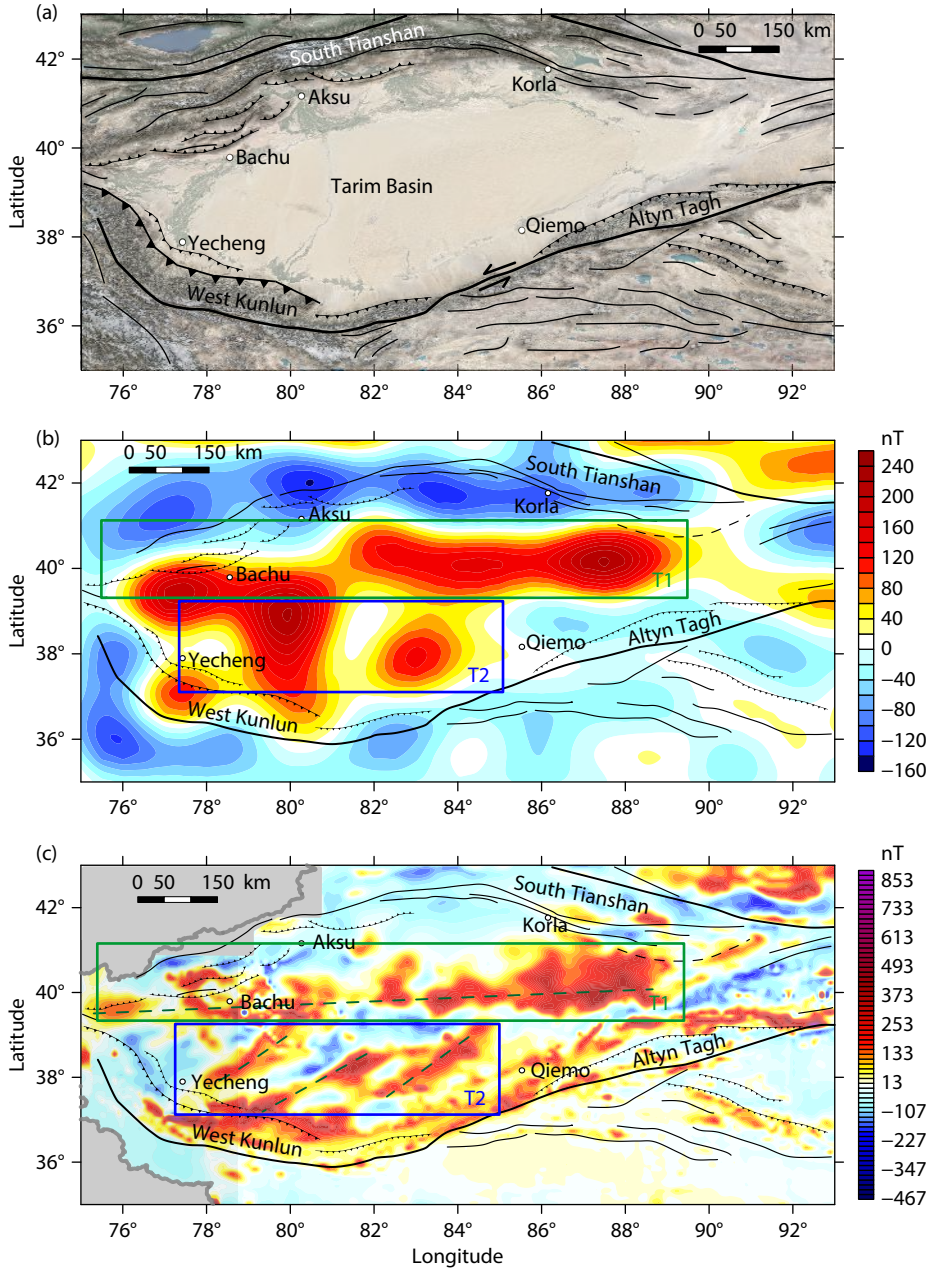

Figure 5. (a) Simplified tectonic map in the Tarim Basin. (b) RTP Tarim magnetic anomaly at Earth's surface, via CHAOS-7 model. (c) RTP aeromagnetic anomaly in Tarim Basin. The green and blue boxes show two divisions of anomalies, T1 and T2, in different trendings.

of the basement.

The Tarim magnetic anomaly was first noticed in aeromagnetic surveys, as long ago as the 1950s. The aeromagnetic anomaly in the Tarim Basin is a broad anomaly, quite similar in spatial distribution to the satellite-observed anomaly, which indicates that the magnetic sources in Tarim Basin are located in the deep crust; even in near-surface aeromagnetic surveys the Tarim magnetic anomaly lacks short-wavelength detail. Many researchers have used these aeromagnetic observations to study the evolution of the Tarim Basin (Gao GM et al., 2015; Wu GH et al., 2020; Xu X et al., 2021). On the aeromagnetic anomaly map (Figure 5c), the Tarim magnetic anomaly could be further divided into two groups of magnetic anomalies based on their different trendings: (1) T1: the broad E-W trending anomaly across the middle of the Tarim Basin, bounded by the green box and (2) T2: the parallel NE-SW trending anomalies in the southern part of the Tarim basin, bounded by the blue box. T1 is considered to be a suture zone that separated the north and south parts of the Tarim Basin during the Precambrian (Xu ZQ et al., 2013). Disputes regarding the T1's origin focus mainly on when it was formed — Paleoproterozoic (Wu GH et al., 2020) or Neoproterozoic (Guo ZJ et al., 2001; Wu GY et al., 2006). Compared to the T1 anomaly, T2 is relatively poorly understood; its origin, also, is not clear. Wang YC et al. (1994) considered that T1 and T2 have a common origin because of their similarities of scale and spatial connection, and that the T2 pair of anomalies are likely to be branches of T1. Guo ZJ et al. (2001) proposed that the T2 were formed earlier than T1, for the reason that they do not across the T1 further north.

Besides, borehole rock samples collected from the basement are limited because of the thick sedimentary cover, and among the few basement granitic samples, from both the Paleoproterozoic and Neoproterozoic, no rock magnetism data have been reported. Thus, due to the difficulty of accessing the basin basement, it remains difficult to draw conclusions about the formation time of the Tarim magnetic anomaly.

3.2 SC: Sichuan Basin

The Sichuan Basin magnetic anomaly is the most striking anomaly in South China. It occupies the whole Sichuan Basin and extends continuously more than 1000 km. On the aeromagnetic anomaly map (Figure 6) it is also characterized by a large-scale linear magnetic anomaly of broad width — ca. 100 km. The geological setting and anomaly characteristics of the Sichuan Basin are very similar to those of the Tarim Basin. The Sichuan magnetic anomaly also reveals the magnetization difference of the basement, and it has attracted the interests of many researchers to study its origin (Luo, 1998; Gu ZD and Wang ZC, 2014; Xiong XS et al., 2015; Wang J et al., 2020a). However, its basement is covered by 4–10 km of layered sedimentary successions from late Neoproterozoic to Cenozoic (Dong SW et al., 2013; Gao R et al., 2016); this thick non-magnetic layer conceals the magnetic sources in the Sichuan Precambrian basement, making it difficult to explore the geological origins of this magnetic anomaly. There are no data from drilling in the magnetic anomaly region that might help determine properties of the strongly magnetized rocks in the Sichuan basement.

We compared the Sichuan Basin satellite RTP magnetic anomaly to surrounding faults, and found obvious correlation in spatial distribution: the magnetic anomaly distribution is bounded by the surrounding faults. Compared to the total-field magnetic anomaly (Figure 6c), the location of the RTP magnetic anomaly (Figure 6d) migrates northward ca. 50 km; the magnetic low accompanying the magnetic high on the north decreases significantly and the shape of the magnetic high becomes more symmetrical. Before RTP correction, the correlation between anomaly distribution and faults is not clear, due to the position offsets caused by oblique magnetization. Recently, Wang J et al. (2020a) applied quantitative 3D inversion (Li YG and Oldenburg, 1996) constrained by the Curie depth as the magnetic source bottom to convert the aeromagnetic grid data into a sub-surface susceptibility model; they found that the spatial distribution of the Sichuan Basin magnetic source controls the range of the rigid basement beneath Sichuan Basin. Combined with geological data, this conclusion led them to propose that the formation of the Sichuan Basin magnetic anomaly might be related to a Precambrian tectono-thermal event that played an important role in stabilizing the Sichuan Basin basement.

3.3 GX: Great Xing'an Range

There is a magnetic high anomaly located over northeast China, a transitional area between the Paleo-Asian tectonic domain and the Circum-Pacific tectonic domain. Figure 7 illustrates the RTP magnetic anomaly over northeast China at different altitudes from Earth's surface to 500 km, as calculated using the CHAOS-7 model. At 500 km and 300 km altitudes, this magnetic high appears to occupy the entire Great Xing'an Range and Songliao Basin, but the anomaly's center is over Great Xing'an Range. After downward continuation to 100 km altitude, the calculated

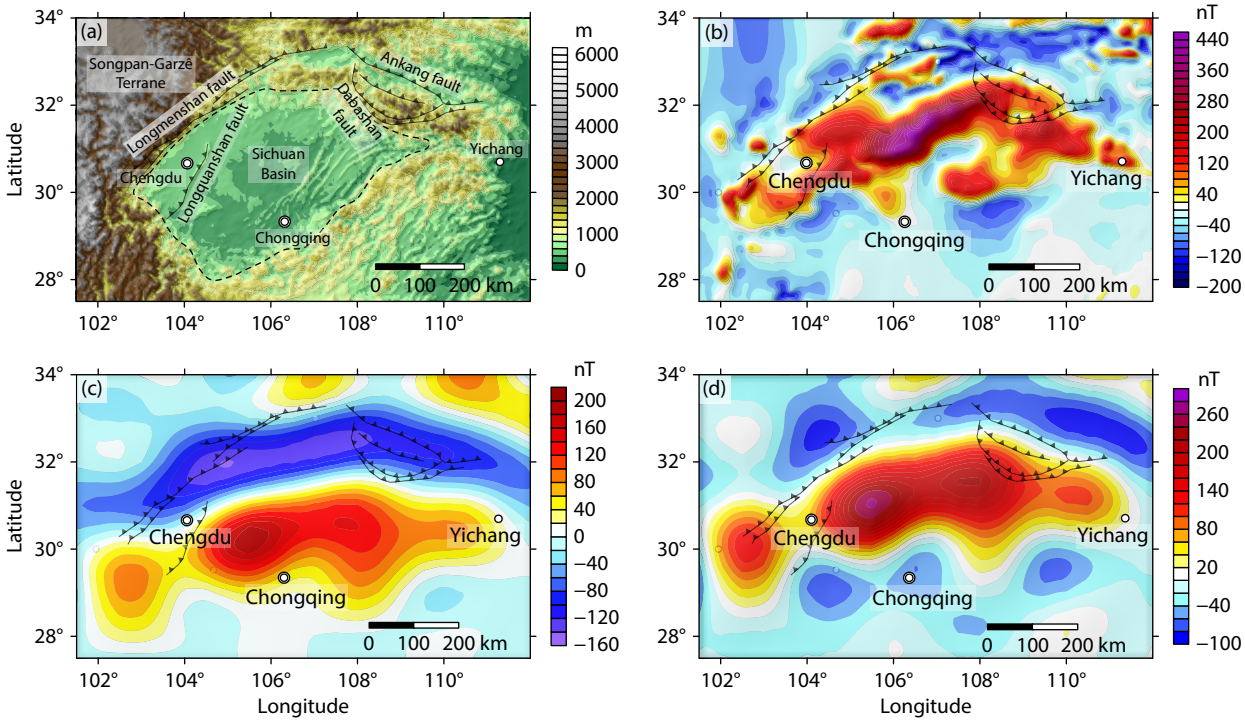

Figure 6. (a) Topography in the Sichuan Basin, modified from Wang J et al. (2020a). (b) RTP aeromagnetic anomaly in the Sichuan Basin. (c) Total-field and (d) RTP magnetic anomaly of CHAOS-7 model at Earth's surface in Sichuan Basin. The main thrust faults have been overlaid to each magnetic anomaly.

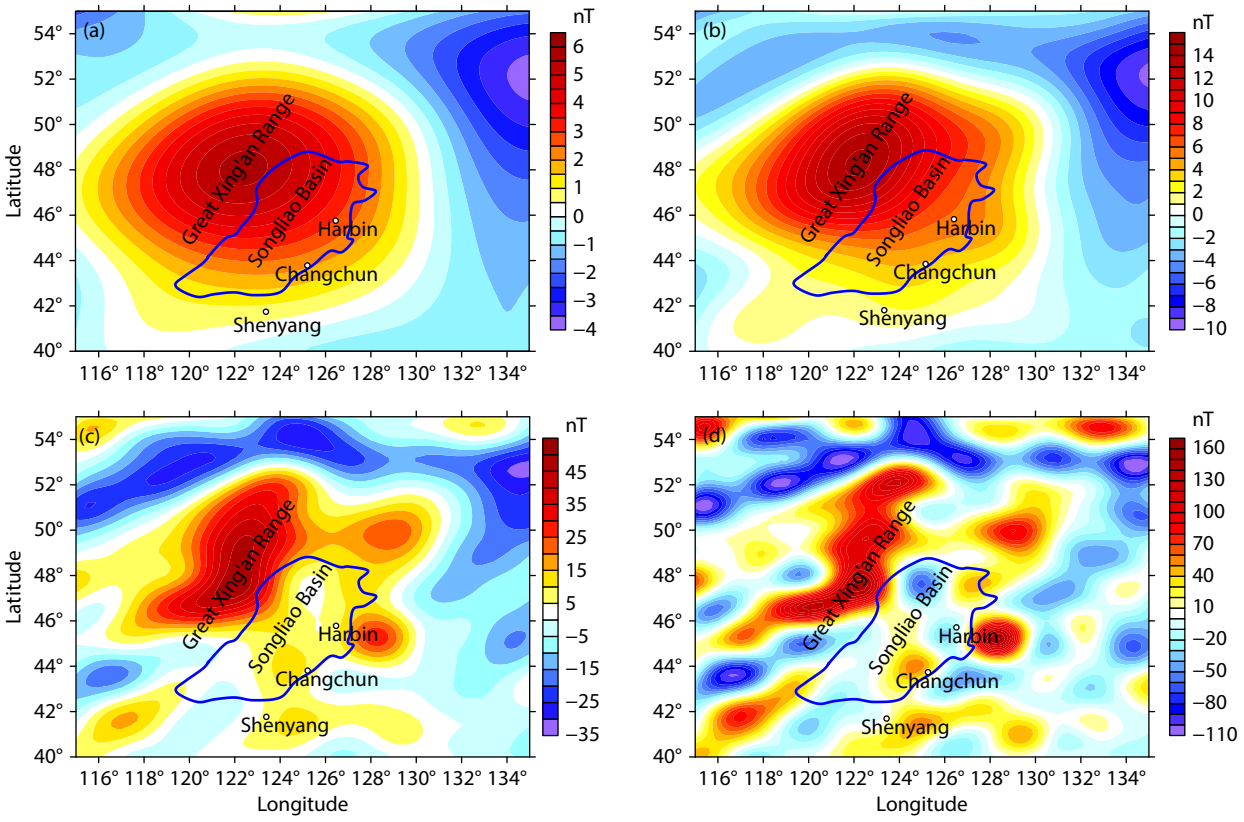

Figure 7. Great Xing'an Range RTP magnetic anomalies, via CHAOS-7 model, at (a) 500 km altitude, (b) 300 km altitude, (c) 100 km altitude and (d) Earth's surface. The blue curves represent the range of the Songliao Basin.

magnetic anomaly separates into a series of relatively small-scale magnetic anomalies, as well as a major anomaly that is now clearly associated with the Great Xing'an Range (Wang J and Li CF, 2018). At the Earth's surface, more details of the Great Xing'an Range anomaly emerge — an NNE trending in the north part, and an E-W trending in the south part. The magnetic anomaly's features obtained from the satellite data are similar to those detected by the aeromagnetic method (Hu XZ et al., 2006): within the Songliao Basin, the aeromagnetic anomaly is relatively smooth with the value of −200 to 300 nT; in the northwestern Great Xing'an Range region, the aeromagnetic anomaly changes severely, with a very high positive amplitude, larger than 1000 nT. The aeromagnetic anomaly of northeast China is mainly NE-NNE and striking near EW, with NNE being the dominant direction. The NE-NNE trending of the anomaly matches the Meso-Cenozoic Pacific plate subduction, and the EW striking anomaly closely reflects the collision and collage between the Siberia and the North China plates. Mesozoic volcanism is widespread throughout northeastern China, which can be subdivided into six stages from Late Triassic to Late Cretaceous (Wang F et al., 2006; Xu WL et al., 2013). Their spatial distribution correlates obviously with the detected magnetic anomalies over the Great Xing'an Range, indicating that the magnetic source could quite plausibly be the Mesozoic magmatic rocks.

3.4 HT: Himalayan-Tibetan Plateau

The magnetic low detected over the southern Himalayan-Tibetan plateau and part of the northwestern region of the Indian shield, has a wide spatial range with an E-W direction, which is parallel to the trending of the tectonic sutures formed by N-S subduction and collision between the Asian and Indian plates. The Himalayan–Tibetan Plateau consists of a set of accreted terranes. Continent–continent collision since the Paleocene thickened the Himalayan–Tibetan crust to double–normal–thickness, resulting in the enormous uplifts of the Himalayan–Tibetan Plateau.

Arkani-Hamed et al. (1988) produced a magnetic anomaly map of China using Magsat data collected over China, and noted that the pronounced low magnetic susceptibility of Tibet is consistent with the thick upper crust and with the observed evidence of high heat flow, suggesting that the Curie isotherm has been displaced upward and that part of the highly magnetic lower crust has been thermally demagnetized. To study this large negative anomaly in the Indo Eurasian collision zone, Rajaram and Langel (1992) also used Magsat data and modeled this region by introducing magnetic blocks representing the Tibetan, Asian and Himalayan mountain regions; they suggested two possible explanations: one, that the origin and tectonic history of the Tibetan region differs from neighboring regions, resulting in lower susceptibility; the other, that the Curie isotherm in the Tibetan region is elevated compared to the Asian and Himalayan regions. Alsdorf and Nelson (1999) applied forward modeling to the magnetic low with six Magsat tracks across the Tibetan plateau, which suggested that the Curie isotherm is likely to reside in the upper crust across the Tibetan plateau and that the raised Curie-isotherm caused the magnetic low. Hemant and Mitchell (2009) forward modeled the

wide magnetic low anomaly within the Himalayan–Tibetan orogen and the Gangetic Plains by introducing a priori geological and geophysical information with depth; their approach, too, indicated that the source of the observed anomaly resides in the upper crust and that much of the middle and lower crust appears non-magnetic due to the elevated Curie isotherm.

All the above-mentioned interpretations of the magnetic low call for a weak magnetized middle-to-lower crust because of the shallow Curie isotherm, which is consistent with the deep crustal structure reflected by the seismic and magnetotelluric experiments conducted across southern Tibet; they have revealed a low-velocity and high-conductivity zone with its top at a depth of 15–20 km, interpreted as being in a partial melting zone in the middle crust (Zhao WJ et al., 1993; Wei WB et al., 2001; Unsworth et al., 2005).

3.5 BM: Barmer Basin

Much less study has been done on the magnetic high anomaly over the northwest of India; no aeromagnetic data from the northern part of India are available (Rajaram et al., 2009). So, to analyze this anomaly we have done some direct comparison with the region's tectonic map. In Figure 8, we present the long-wavelength magnetic anomaly as calculated by applying the CHAOS-7 model at Earth's surface after RTP, overlaid in the figure by the tectonic divisions in this area. The magnetic anomaly is approximately N-S trending, centered near the Barmer Basin. The Barmer Basin preserves a thick Neoproterozoic to Miocene stratigraphy overlain by Quaternary deposits. At least 6 km of Jurassic-to-recent deposits overlie the Neoproterozoic basement (Najman et al., 2018), similar to the Tarim and Sichuan Basin in China, which have a thick sedimentary layer from the Neoproterozoic and a long-lived Precambrian basement. However, this Indian area is a tectonic fracture zone due to the far-field effects of the Indian-Asian collision. The Indian plate is under N-S compressive stress from the forces of the central Indian Ocean mid-ocean ridge and the Tibetan Plateau. It is difficult to correlate the magnetic anomaly directly with surficial features in such a complex setting. To determine the origin of this magnetic anomaly, further detailed study and field surveys, combined with geological data, will be necessary.

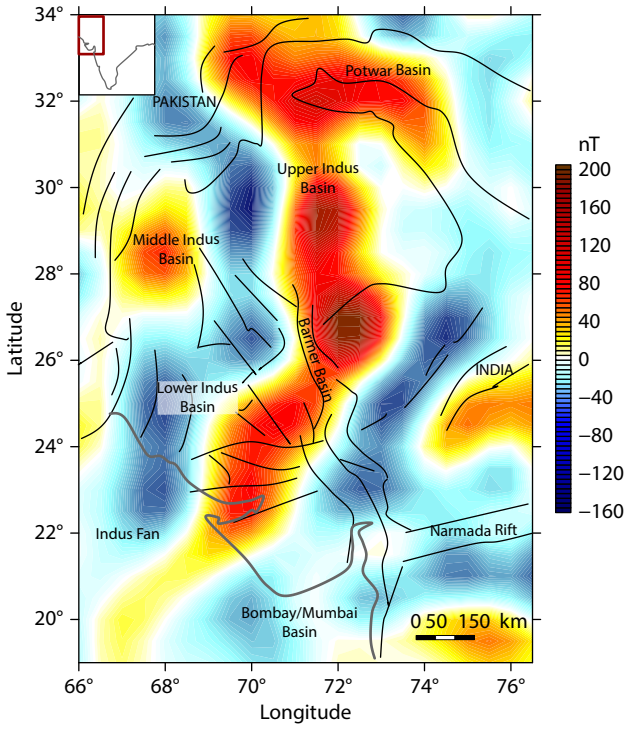

Figure 8. Barmer Basin RTP magnetic anomaly at Earth's surface (via CHAOS-7 model). The tectonic lines of northwest India are simplified from Najman et al. (2018).

3.6 CM: Central Myanmar Basin

The single long-wavelength magnetic anomaly over Myanmar at 500 km altitude divides into a series of relatively small-scale anomalies after downward continuation closer to the Earth's surface. Because no near-surface magnetic data are currently available for this area, we have done some comparison directly between the satellite RTP magnetic anomaly on Earth's surface, and the region's tectonic map (Figure 9). The region's magnetic anomalies with long-wavelength constituents are mainly distributed in a N-S trending over the Central Myanmar Basin, between the Indo-Burma Ranges and the Shan Plateau, located at the southern edge of the eastern Himalayan syntaxis and follow the ongoing continental collision between Indian and Burmese (belonging to the Eurasian side) plates. The N-S trending Wuntho-Popa arc divides the Central Myanmar Basin into a western forearc basin and an eastern back-arc basin (Cai FL et al., 2020; Ye Htut et al., 2020). The magnetic anomalies are mainly over the forearc basin side. Blakely et al. (2005) suggested that serpentinized mantle wedge in forearc settings, cooled by subduction, should contribute to long-wavelength magnetic anomalies above subduction zones. The Wuntho-Popa arc is a Neo-Tethyan arc,

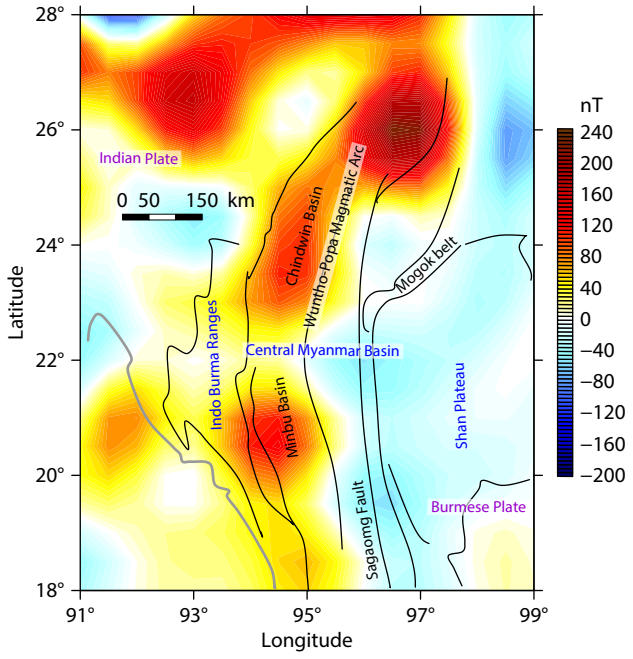

Figure 9. Central Myanmar Basin RTP magnetic anomaly at Earth's surface, via CHAOS-7 model. The tectonic lines are simplified from Cai FL et al. (2020).

resembling the giant Gangdese arc along the Yarlung-Zangbo suture zone in southern Tibet, which also has strong aeromagnetic anomalies caused by a mafic magmatic root beneath the granitic batholith (Wang J et al., 2020b). A serpentinized mantle wedge or deep magnetic magmatic root both could be possible sources for this magnetic anomaly.

3.7 SD: Sunda and Banda Arcs

A striped magnetic anomaly extends along the Sunda and Banda arcs in Indonesia. The Sunda and Banda arcs were formed during the northward subduction of the Indo-Australian plate, resulting in a quite complex tectonic setting. In the east, the Australian plate has been colliding with the Banda arc since about 5 Ma; whereas, to the west, the oceanic part of the Indo-Australian plate is still subducting beneath the Java trench. The age of the subducting ocean floor varies from 50–90 Ma along Sumatra to 100–135 Ma and 140–160 Ma near Java and Flores, respectively (Widiyantoro and van der Hilst, 1996).

Zubaidah et al. (2010, 2014) carried out several geomagnetic ground surveys in the Lombok Island, part of the Lesser Sunda Islands, and generated new integrated magnetic-gravity forward models. They interpreted this strong magnetic anomaly to be caused by a serpentinized forearc magnetic mantle of the Flores Thrust subduction zone, another southward subducting slab. The Flores Thrust lies to the north of the volcanic arcs; it has been considered to be as a newly formed back arc trench that probably resulted from the Indian oceanic slab break-off. This would mean that two subduction domains exist in this area: the northward subducting Indian slab and the southward subducting Flores slab. Because Zubaidah et al. (2014) did not provide the RTP magnetic anomaly map in this area, we have used the CHAOS-7 model to picture (Figure 10) the total-field and RTP magnetic anomaly from Jave to the Flores islands, where the magnetic anomaly is relatively strong. The latitude of this anomaly is relatively low; the conventional RTP methods are unstable at low altitudes and cause obvious stripe error in north-south trending; moreover, false high-frequency signals make the maximum value appear to be increasing from 250 nT to 381 nT (Figure 10c). So, we undertook the RTP with suppression filter (Yao CL et al., 2003) to improve the low-latitude RTP result (Figure 10d); the north–south stripe error is significantly suppressed compared to Figure 10c, and the maximum value is reduced to a reasonable level, 239 nT. After RTP, the magnetic anomaly is seen to migrate southward about 100 km, moving to the south of the volcanic arc, which suggests that the magnetic anomaly source is not in the forearc part of the Flores Thrust subduction zone; on the contrary, it is more likely to be located in the forearc part of the northward subducting Indian oceanic plate, rather than the southward Flores subduction zone. Based on existing analysis, it remains difficult to determine to which subduction zone the magnetic courses can be attributed. To locate the source of the long-wavelength magnetic anomaly in this complex subduction zone more clearly, more detailed near-surface magnetic surveys are needed.

4. Conclusions

Satellite magnetic surveys provide high-quality magnetic data for study of large-scale regional tectonics. But at 500 km altitude, most small-scale magnetic anomalies disappear; only long-wavelength anomalies can be detected by satellite at that altitude. In China and surrounding regions, there are six magnetic high and one magnetic low long-wavelength magnetic anomalies detected in satellite data. The tectonic backgrounds for these anomalies are related to either ancient basin basement or subduction-collision

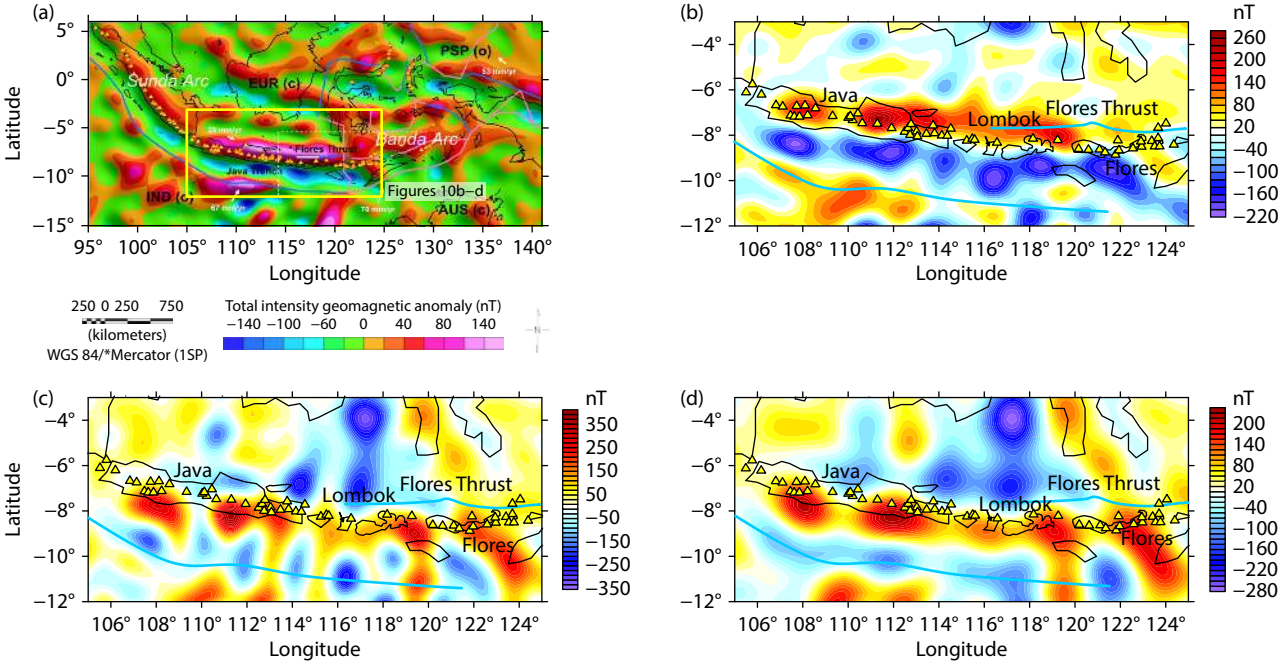

Figure 10. (a) Total-field magnetic anomaly (via the MF7 model) in Indonesia, modified from Zubaidah et al. (2014). The yellow box shows the location of the subregion shown in Figures 10b–d. (b) Total field, (c) Conventional RTP and (d) low-latitude RTP with suppression filter magnetic anomaly from Java to Flores islands at Earth's surface, via CHAOS-7 model. The yellow triangles indicate the locations of volcanos.

zone:

(1) **TR, SC and BM (ancient basin basement)**: The magnetic anomalies over TR and SC in China are still large-scale near the surface, suggesting that these anomalies have deep sources. They have very similar geological settings — Precambrian rigid basement and thick sedimentary layers from the Neoproterozoic. Coincidentally, the magnetic anomaly in the northwest of India is also centered on BM with similar background, but smaller in spatial scale. The magnetic anomaly over the northwest of India divides into several small anomalies after downward continuation to the surface, unlike the magnetic anomaly over the TR and SC which remain large-scale.

(2) **GX, HT, CM and SD (subduction-collision zone)**: It is clear that the long-wavelength magnetic anomalies in the SD and CM are associated with subduction zones, but further discussion is still needed to decide whether these magnetic anomalies are caused by magmatic arc intrusions or by serpentinized mantle wedge. The GX is in a transitional area between the Paleo-Asian tectonic domain and the Meso-Cenozoic Pacific plate subduction zone, with widespread exposure of Mesozoic volcanic rocks. The HT is a striking magnetic low caused by its shallow Curie depth due to high heat flow generated by the ongoing collision between the Asian and Indian plates.

Geological origins of long-wavelength magnetic anomalies are always debatable. The difficulties of geological and tectonic interpretation come mainly from the following:
(1) limited exposure. Long-wavelength magnetic anomalies are most probably caused by deep-seated sources, but strongly-magnetized basement rocks often have limited surficial exposure, especially in ancient cratons, which are often covered by thick non-magnetic sedimentary layers and thus exhibit no obvious correlation between the magnetic anomaly and surficial features (e.g., TR, SC, BM);
(2) tectonic destruction. In tectonic fracture zones, the crustal fragmentation and movement due to later tectonic forces increase the difficulty of identifying corresponding geological bodies (e.g., BM, CM, SD);
(3) multi-phase superposition. A lithospheric magnetic anomaly has, itself, only spatial attributes, not temporal attributes. What we observe is a comprehensive reflection of all activities that took place during geological history. Such a superposition of multiple tectonic activities makes it difficult to determine which geological event is most related to the anomaly formation (e.g., TR, SC, GX).

In an interpretation of long-wavelength magnetic anomaly data, careful consideration of the complexity of deep physical properties and structures, caused by tectonic destruction and superimposed multi-phase geological events, must be considered; magnetic forward and inversion modeling, combined with deep constraints from other means (e.g., deep seismic reflection, magnetotelluric, thermal structure, rock magnetism) would be helpful in any quantitative analysis of a magnetic anomaly.

Acknowledgments

This work was supported by the National Natural Science Foundation of China (grant numbers 42004051, 42274214, 41904134).

References

Alsdorf, D., and Nelson, D. (1999). Tibetan satellite magnetic low: evidence for widespread melt in the Tibetan crust?. *Geology, 27*(10), 943–946. https://doi.org/10.1130/0091-7613(1999)027<0943:TSMLEF>2.3.CO;2

An, Z. C., Ma, S. Z., Tan, D. H., Barraclough, D. R., and Kerridge, D. J. (1992). A spherical cap harmonic model of the satellite magnetic anomaly field over China and adjacent areas. *J. Geomagn. Geoelectr., 44*(3), 243–252. https://doi.org/10.5636/jgg.44.243

Arkani-Hamed, J., Zhao, S. K., and Strangway, D. W. (1988). Geophysical interpretation of the magnetic anomalies of China derived from *Magsat* data. *Geophys. J. Int., 95*(2), 347–359. https://doi.org/10.1111/j.1365-246X.1988.tb00473.x

Arkani-Hamed, J., Langel, R. A., and Purucker, M. (1994). Scalar magnetic anomaly maps of Earth derived from POGO and Magsat data. *J. Geophys. Res.: Solid Earth*, *99*(B12), 24075–24090. https://doi.org/10.1029/94jb00930

Blakely, R. J. (1995). *Potential Theory in Gravity and Magnetic Applications*. Cambridge: Cambridge University Press.

Blakely, R. J., Brocher, T. M., and Wells, R. E. (2005). Subduction-zone magnetic anomalies and implications for hydrated forearc mantle. *Geology*, *33*(6), 445–448. https://doi.org/10.1130/G21447.1

Cai, F. L., Ding, L., Zhang, Q. H., Orme, D. A., Wei, H. H., Li, J. X., Zhang, J. E., Zaw, T., and Sein, K. 2020. Initiation and evolution of forearc basins in the Central Myanmar Depression. *GSA Bull., 132*(5-6), 1066–1082. https://doi.org/10.1130/B35301.1

Dong, S. W., Gao, R., Yin, A., Guo, T. L., Zhang, Y. Q., Hu, J. M., Li, J. H., Shi, W., and Li, Q. S. (2013). What drove continued continent-continent convergence after ocean closure? Insights from high-resolution seismic-reflection profiling across the Daba Shan in central China. *Geology*, *41*(6), 671–674. https://doi.org/10.1130/G34161.1

Du, J. S. (2014). Study on processing, forward modeling and inversion algorithms of satellite magnetic anomaly data in spherical coordinate system [Ph. D. thesis] (in Chinese). Wuhan: China University of Geosciences.

Ferré, E. C., Friedman, S. A., Martín-Hernández, F., Feinberg, J. M., Till, J. L., Ionov, D. A., and Conder, J. A. (2014). Eight good reasons why the uppermost mantle could be magnetic. *Tectonophysics, 624-625*, 3–14. https://doi.org/10.1016/j.tecto.2014.01.004

Finlay, C. C., Kloss, C., Olsen, N., Hammer, M. D., Tøffner-Clausen, L., Grayver, A., and Kuvshinov, A. (2020). The CHAOS-7 geomagnetic field model and observed changes in the South Atlantic Anomaly. *Earth, Planets Space, 72*(1), 156. https://doi.org/10.1186/s40623-020-01252-9

Finn, C. A., Goodge, J. W., Damaske, D., and Fanning, C. M. (2006). Scouting craton's edge in paleo-pacific gondwana. In D. K. Fütterer, et al. (Eds.), *Antarctica: Contributions to Global Earth Sciences* (pp. 165-173). Berlin Heidelberg: Springer. https://doi.org/10.1007/3-540-32934-X_20

Friis-Christensen, E., Lühr, H., and Hulot, G. (2006). *Swarm*: a constellation to study the earth's magnetic field. *Earth, Planets Space, 58*(4), 351–358. https://doi.org/10.1186/BF03351933

Gao, G. M., Kang, G. F., Li, G. Q., and Bai, C. H. (2015). Crustal magnetic anomaly and Curie surface beneath Tarim Basin, China, and its adjacent area. *Can. J. Earth Sci., 52*(6), 357–367. https://doi.org/10.1139/cjes-2014-0204

Gao, G. M., Shi, L., Kang, G. F., Wu, Y. Y., Bai, C. H., Wen, L. M., and Hou, J. (2018). Analysis of the lithospheric magnetic anomalies and tectonics in continental China and the adjacent regions using CHAMP satellite data. *Stud. Geophys. Geod., 62*(3), 408–426. https://doi.org/10.1007/s11200-016-0102-7

Gao, R., Chen, C., Wang, H. Y., Lu, Z. W., Brown, L., Dong, S. W., Feng, S. Y., Li, Q. S., Li, W. H., … Li, F. (2016). SINOPROBE deep reflection profile reveals a Neo-Proterozoic subduction zone beneath Sichuan Basin. *Earth Planet. Sci. Lett., 454*, 86–91. https://doi.org/10.1016/j.epsl.2016.08.030

Girdler, R. W., Taylor, P. T., and Frawley, J. J. (1992). A possible impact origin for the Bangui magnetic anomaly (Central Africa). *Tectonophysics*, *212*(1-2), 45–58. https://doi.org/10.1016/0040-1951(92)90139-W

Goodge, J. W., and Finn, C. A. (2010). Glimpses of East Antarctica: aeromagnetic and satellite magnetic view from the central transantarctic mountains of East Antarctica. *J. Geophys. Res.: Solid Earth*, *115*(B9), B09103. https://doi.org/

10.1029/2009JB006890

Gu, Z. D., and Wang, Z. C. (2014). The discovery of Neoproterozoic extensional structures and its significance for gas exploration in the Central Sichuan Block, Sichuan basin, South China. *Sci China Earth Sci.*, *57*(11), 2758–2768. https://doi.org/10.1007/s11430-014-4961-x

Guo, Z. J., Zhang, Z. C., Jia, C. Z., and Wei, G. Q. (2001). Tectonics of Precambrian basement of the Tarim craton. *Sci. China Ser. D: Earth Sci.*, *44*(3), 229–236. https://doi.org/10.1007/BF02882257

He, B. Z., Jiao, C. L., Cai, Z. H., Zhang, M., and Gao, A. R. (2011). A new interpretation of the high aeromagnetic anomaly zone in central Tarim Basin. *Geol. China (in Chinese)*, *38*(4), 961–969. https://doi.org/10.3969/j.issn.1000-3657.2011.04.013

Hemant, K., and Maus, S. (2005). Geological modeling of the new CHAMP magnetic anomaly maps using a geographical information system technique. *J. Geophys. Res.: Solid Earth*, *110*(B12), B12103. https://doi.org/10.1029/2005JB003837

Hemant, K., and Mitchell, A. (2009). Magnetic field modelling and interpretation of the Himalayan–Tibetan Plateau and adjoining north Indian Plains. *Tectonophysics*, *478*(1-2), 87–99. https://doi.org/10.1016/j.tecto.2009.06.009

Hu, X. Z., Xu, M. J., Xie, X. A., Wang, L. S., Zhang, Q. L., Liu, S. W., Xie, G. A., and Feng, C. G. (2006). A characteristic analysis of aeromagnetic anomalies and Curie point isotherms in Northeast China. *Chin. J. Geophys. (in Chinese)*, *49*(6), 1674–1681. https://doi.org/10.3321/j.issn:0001-5733.2006.06.014

Huang, J. P., Shen, X. H., Zhang, X. M., Lu, H. X., Tan, Q., Wang, Q., Yan, R., Chu, W., Yang, Y. Y., … Xu, S. (2018). Application system and data description of the China Seismo-Electromagnetic Satellite. *Earth Planet. Phys.*, *2*(6), 444–454. https://doi.org/10.26464/epp2018042

Ingram, G. M., Chisholm, T. J., Grant, C. J., Hedlund, C. A., Stuart-Smith, P., and Teasdale, J. (2004). Deepwater North West Borneo: hydrocarbon accumulation in an active fold and thrust belt. *Mar. Pet. Geol.*, *21*(7), 879–887. https://doi.org/10.1016/j.marpetgeo.2003.12.007

Kang, G. F., Gao, G. M., Bai, C. H., Wang, J., and Shao, D. (2010). Distribution of the magnetic anomaly for the CHAMP satellite in China and adjacent areas. *Chin. J. Geophys. (in Chinese)*, *53*(4), 895–903. https://doi.org/10.3969/j.issn.0001-5733.2010.04.014

Langel, R. A., Phillips, J. D., and Horner, R. J. (1982). Initial scalar magnetic anomaly map from MAGSAT. *Geophys. Res. Lett.*, *9*(4), 269–272. https://doi.org/10.1029/GL009i004p00269

Langel, R. A., and Hinze, W. J. (1998). *The Magnetic Field of the earth's Lithosphere: The Satellite Perspective*. Cambridge: Cambridge University Press.

Li, Y. G., and Oldenburg, D. W. (1996). 3-D inversion of magnetic data. *Geophysics*, *61*(2), 394–408. https://doi.org/10.1190/1.1443968

Luo, Z. L. (1998). New recognition of basement in Sichuan Basin. *J. Chengdu Univ. Technol. (in Chinese)*, *25*(2), 191–200.

Maus, S., Rother, M., Holme, R., Lühr, H., Olsen, N., and Haak, V. (2002). First scalar magnetic anomaly map from CHAMP satellite data indicates weak lithospheric field. *Geophys. Res. Lett.*, *29*(14), 1702. https://doi.org/10.1029/2001gl013685

Maus, S., Yin, F., Lühr, H., Manoj, C., Rother, M., Rauberg, J., Michaelis, I., Stolle, C., and Müller, R. D. (2008). Resolution of direction of oceanic magnetic lineations by the sixth-generation lithospheric magnetic field model from CHAMP satellite magnetic measurements. *Geochem., Geophys., Geosyst.*, *9*(7), Q07021. https://doi.org/10.1029/2008GC001949

Najman, Y., Burley, S. D., Copley, A., Kelly, M. J., Pander, K., and Mishra, P. (2018). The late Eocene-early Miocene unconformities of the NW Indian intraplate basins and Himalayan foreland: a record of tectonics or mantle dynamics?. *Tectonics, 37*(10), 3970-3985. https://doi.org/10.1029/2018TC005286

Olsen, N., Ravat, D., Finlay, C. C., and Kother, L. K. (2017). LCS-1: a high-resolution global model of the lithospheric magnetic field derived from CHAMP and *Swarm* satellite observations. *Geophys. J. Int.*, *211*(3), 1461–1477. https://doi.org/10.1093/GJI/GGX381

Ou, J. M., Du, A. M., Thébault, E., Xu, W. Y., Tian, X. B., and Zhang, T. L. (2013). A high resolution lithospheric magnetic field model over China. *Sci. China Earth Sci.*, *56*(10), 1759–1768. https://doi.org/10.1007/s11430-013-4580-y

Purucker, M., Langlais, B., Olsen, N., Hulot, G., and Mandea, M. (2002). The southern edge of cratonic North America: evidence from new satellite magnetometer observations. *Geophys. Res. Lett.*, *29*(15), 8000. https://doi.org/10.1029/2001GL013645

Purucker, M. E., and Clark, D. A. (2011). Mapping and interpretation of the lithospheric magnetic field. In M. Mandea, et al. (Eds.), *Geomagnetic Observations and Models* (pp. 311-337). Dordrecht: Springer. https://doi.org/10.1007/978-90-481-9858-0_13

Rajaram, M., and Langel, R. A. (1992). Magnetic anomaly modeling at the Indo Eurasian collision zone. *Tectonophysics*, *212*(1-2), 117–127. https://doi.org/10.1016/0040-1951(92)90144-U

Rajaram, M., Anand, S. P., Hemant, K., and Purucker, M. E. (2009). Curie isotherm map of Indian subcontinent from satellite and aeromagnetic data. *Earth Planet. Sci. Lett.*, *281*(3-4), 147–158. https://doi.org/10.1016/j.epsl.2009.02.013

Ravat, D., Langel, R. A., Purucker, M., Arkani-hamed, J., and Alsdorf, D. E. (1995). Global vector and scalar Magsat magnetic anomaly maps. *J. Geophys. Res.: Solid Earth*, *100*(B10), 20111–20136. https://doi.org/10.1029/95JB01237

Ravat, D. N., Hinze, W. J., and Taylor, P. T. (1993). European tectonic features observed by Magsat. *Tectonophysics*, *220*(1-4), 157–173. https://doi.org/10.1016/0040-1951(93)90229-D

Regan, R. D., Davis, W. M., and Cain, J. C. (1973). The Bangui magnetic anomaly (abstract). *Eos Trans. AGU*, *54*(4), 236.

Regan, R. D., Cain, J. C., and Davis, W. M. (1975). A global magnetic anomaly map. *J. Geophys. Res.*, *80*(5), 794–802. https://doi.org/10.1029/JB080i005p00794

Regan, R. D., and Marsh, B. D. (1982). The Bangui magnetic anomaly: Its geological origin. *J. Geophys. Res.: Solid Earth*, *87*(B2), 1107–1120. https://doi.org/10.1029/JB087iB02p01107

Sabaka, T. J., Tøffner-Clausen, L., Olsen, N., and Finlay, C. C. (2020). CM6: a comprehensive geomagnetic field model derived from both CHAMP and Swarm satellite observations. *Earth Planets Space*, *72*(1), 80. https://doi.org/10.1186/s40623-020-01210-5

Shen, X. H., Zhang, X. M., Yuan, S. G., Wang, L. W., Cao, J. B., Huang, J. P., Zhu, X. H., Piergiorgio, P., and Dai, J. P. (2018). The state-of-the-art of the China Seismo-Electromagnetic Satellite mission. *Sci. China Technol. Sci.*, *61*(5), 634–642. https://doi.org/10.1007/s11431-018-9242-0

Taylor, P. T., and Frawley, J. J. (1987). Magsat anomaly data over the Kursk region, U.S.S.R. *Phys. Earth Planet. Inter.*, *45*(3), 255–265. https://doi.org/10.1016/0031-9201(87)90014-8

Taylor, P. T., Kis, K. I., and Wittmann, G. (2014). Satellite-altitude horizontal magnetic gradient anomalies used to define the Kursk Magnetic Anomaly. *J. Appl. Geophys.*, *109*, 133–139. https://doi.org/10.1016/j.jappgeo.2014.07.018

Thébault, E., Vigneron, P., Langlais, B., and Hulot, G. (2016). A Swarm lithospheric magnetic field model to SH degree 80. *Earth Planets Space, 68*(1), 126. https://doi.org/10.1186/s40623-016-0510-5

Unsworth, M. J., Jones, A. G., Wei, W., Marquis, G., Gokarn, S. G., Spratt, J. E., and The INDEPTH-MT Team. (2005). Crustal rheology of the Himalaya and Southern Tibet inferred from magnetotelluric data. *Nature*, *438*(7064), 78–81. https://doi.org/10.1038/nature04154

von Frese, R. R. B., Kim, H. R., Leftwich, T. E., Kim, J. W., and Golynsky, A. V. (2013). Satellite magnetic anomalies of the Antarctic Wilkes Land impact basin inferred from regional gravity and terrain data. *Tectonophysics*, *585*, 185–195. https://doi.org/10.1016/j.tecto.2012.09.009

Wang, F., Zhou, X. H., Zhang, L. C., Ying, J. F., Zhang, Y. T., Wu, F. Y., and Zhu, R. X. (2006). Late Mesozoic volcanism in the Great Xing'an Range (NE China): timing and implications for the dynamic setting of NE Asia. *Earth Planet. Sci. Lett.*, *251*(1-2), 179–198. https://doi.org/10.1016/j.epsl.2006.09.007

Wang, J., and Li, C. F. (2018). Curie point depths in Northeast China and their geothermal implications for the Songliao Basin. *J. Asian Earth Sci.*, *163*, 177–193. https://doi.org/10.1016/j.jseaes.2018.05.026

Wang, J., Yao, C. L., Li, Z. L., Zheng, Y. M., Shen, X. H., Zeren, Z. M., and Liu, W. L. (2020a). 3D inversion of the Sichuan Basin magnetic anomaly in South China and its geological significance. *Earth Planets Space*, *72*(1), 40. https://doi.org/10.1186/s40623-020-01167-5

Wang, J., Yao, C. L., and Li, Z. L. (2020b). Aeromagnetic anomalies in central

Yarlung-Zangbo suture zone (Southern Tibet) and their geological origins. *J. Geophys. Res.: Solid Earth*, *125*(2), e2019JB017351. https://doi.org/10.1029/2019JB017351

Wang, J., Shen, X. H., Yang, Y. Y., Zeren, Z. M., Hulot, G., Olsen, N., Zhou, B., Magnes, W., De Santis, A., … Yu, J. B. (2021). Initial scalar lithospheric magnetic anomaly map of China and surrounding regions derived from CSES satellite data. *Sci. China Technol. Sci.*, *64*(5), 1118–1126. https://doi.org/10.1007/s11431-020-1727-0

Wang, J., Shen, X. H., Yang, Y. Y., Zeren, Z. M., Huang, J. P., Zhao, S. F., Wang, Q., Lu, H. X., and Guo, F. (2023a). The spherical cap harmonic model of lithospheric magnetic anomaly in Chinese region derived from CSES satellite data. *Chin. J. Geophys. (in Chinese)*, *66*(7), 2973–2982. https://doi.org/10.6038/cjg2022Q0857

Wang, J., Shen, X. H., Yang, Y. Y., Zeren, Z. M., Zhou, B., Werner, M., De Santis, A., Huang, J. P., Yao, C. L., … Lammegger, R. (2023b). A global lithospheric magnetic field model between ± 65° latitude derived from CSES satellite scalar data. *Phys. Earth Planet. Inter.*, *340*, 107036. https://doi.org/10.1016/j.pepi.2023.107036

Wang, Y. C., Yang, H., Wang, X. M., and Zheng, B. Q. (1994). Taklamakan Pre-Sinian paleorift and its petroleum potential. *Xinjiang Petrol. Geol. (in Chinese)*, *15*(3), 191–200.

Wei, W. B., Unsworth, M., Jones, A., Booker, J., Tan, H. D., Nelson, D., Chen, L. S., Li, S. H., Solon, K., … Roberts, B. (2001). Detection of widespread fluids in the Tibetan crust by magnetotelluric studies. *Science*, *292*(5517), 716–719. https://doi.org/10.1126/science.1010580

Widiyantoro, S., and van der Hilst, R. (1996). Structure and evolution of lithospheric slab beneath the Sunda Arc, Indonesia. *Science*, *271*(5255), 1566–1570. https://doi.org/10.1126/science.271.5255.1566

Wu, G. H., Yang, S., Meert, J. G., Xiao, Y., Chen, Y. Q., Wang, Z. C., and Li, X. (2020). Two phases of Paleoproterozoic orogenesis in the Tarim Craton: implications for Columbia assembly. *Gondwana Res.*, *83*, 201–216. https://doi.org/10.1016/j.gr.2020.02.009

Wu, G. Y., Li, Y. J., Wang, G. L., Zheng, W., Luo, J. C., and Meng, Q. L. (2006). Volcanic rocks of Jinningian oceanic islands in the Bachu area, western Xinjiang. *Geoscience (in Chinese)*, *20*(3), 361–369. https://doi.org/10.3969/j.issn.1000-8527.2006.03.001

Xiong, X. S., Gao, R., Zhang, J. S., Wang, H. Y., and Guo, L. H. (2015). Differences of structure in mid-lower crust between the eastern and western blocks of the Sichuan basin. *Chin. J. Geophys. (in Chinese)*, *58*(7), 2413–2423. https://doi.org/10.6038/cjg20150718

Xu, W. L., Wang, F., Pei, F. P., Meng, E., Tang, J., Xu, M. J., and Wang, W. (2013). Mesozoic tectonic regimes and regional ore-forming background in NE China: constraints from spatial and temporal variations of Mesozoic volcanic rock associations. *Acta Petrol. Sin. (in Chinese)*, *29*(2), 339–353.

Xu, X., Zuza, A. V., Yin, A., Lin, X. B., Chen, H. L., and Yang, S. F. (2021). Permian plume-strengthened Tarim lithosphere controls the Cenozoic deformation pattern of the Himalayan-Tibetan orogen. *Geology*, *49*(1), 96–100. https://doi.org/10.1130/G47961.1

Xu, Z. Q., He, B. Z., Zhang, C. L., Zhang, J. X., Wang, Z. M., and Cai, Z. H. (2013). Tectonic framework and crustal evolution of the Precambrian basement of the Tarim Block in NW China: New geochronological evidence from deep drilling samples. *Precambrian Res.*, *235*, 150–162. https://doi.org/10.1016/j.precamres.2013.06.001

Yang, S. F., Chen, H. L., Li, Z. L., Li, Y. Q., and Yu, X. (2017). *Early Permian Tarim Large Igneous Province in Northwest China* (pp. 13-18). Hangzhou: Zhejiang University Press.

Yao, C. L., Guan, Z. N., Gao, D. Z., Zhang, X. L., and Zhang, Y. W. (2003). Reduction-to-the-pole of magnetic anomalies at low latitude with suppression filter. *Chin. J. Geophys. (in Chinese)*, *46*(5), 690–696. https://doi.org/10.3321/j.issn:0001-5733.2003.05.017

Ye Htut, T., Qin, K. Z., Li, G. M., Sein, K., and Evans, N. J. (2020). Eocene arc magmatism and related Cu-Au (Mo) mineralization in the Shangalon-Kyungalon district, Wuntho-Popa Arc, northern Myanmar. *Ore Geol. Rev.*, *125*, 103678. https://doi.org/10.1016/j.oregeorev.2020.103678

Zhang, C. D. (2003). Deduction of magnetic characteristics of lithosphere in China from results on satellite and aeromagnetic measurements. *Prog. Geophys. (in Chinese)*, *18*(1), 103–110. https://doi.org/10.3969/j.issn.1004-2903.2003.01.017

Zhang, K. K. (2023). A novel geomagnetic satellite constellation: science and applications. *Earth Planet. Phys.*, *7*(1), 4–21. https://doi.org/10.26464/epp2023019

Zhao, W. J., Nelson, K. D., Che, J., Quo, J., Lu, D., Wu, C., and Liu, X. 1993. Deep seismic reflection evidence for continental underthrusting beneath Southern Tibet. *Nature, 366*(6455), 557–559. https://doi.org/10.1038/366557a0

Zubaidah, T., Korte, M., Mandea, M., Quesnel, Y., and Kanata, B. (2010). Geomagnetic field anomalies over the Lombok Island region: an attempt to understand the local tectonic changes. *Int. J. Earth Sci.*, *99*(5), 1123–1132. https://doi.org/10.1007/s00531-009-0450-4

Zubaidah, T., Korte, M., Mandea, M., and Hamoudi, M. (2014). New insights into regional tectonics of the Sunda–Banda Arcs region from integrated magnetic and gravity modelling. *J. Asian Earth Sci.*, *80*, 172–184. https://doi.org/10.1016/j.jseaes.2013.11.013